Calculations of Electron Inelastic Mean Free Paths

III. Data for 15 Inorganic Compounds over the 50–2000 eV Range

S. Tanuma

Analysis Research Center, Nippon Mining Company Ltd., 3-17-35 Niizo-Minami, Toda, Saitama 335, Japan

C. J. Powell and D. R. Penn

National Institute of Standards and Technology, Gaithersburg, MD 20899, USA

We report calculations of electron inelastic mean free paths (IMFPs) of 50–2000 eV electrons in a group of 15 inorganic compounds (Al_2O_3, GaAs, GaP, InAs, InP, InSb, KCl, LiF, NaCl, PbS, PbTe, SiC, Si_3N_4, SiO_2 and ZnS). As was found in similar calculations for a group of 27 elements, there are substantial differences in the shapes of the IMFP versus energy curves from compound to compound for energies below 200 eV; these differences are associated with the different inelastic electron scattering characteristics of each material. Comparisons are made of the calculated IMFPs and the values calculated from the predictive IMFP formula TPP-2 developed from the IMFP calculations for the elements. Deviations in this comparison are found, which correlated with uncertainties of the optical data from which the IMFPs were calculated. The TPP-2 IMFP formula is therefore believed to be a more reliable means for determining IMFPs for these compounds than the direct calculations.

INTRODUCTION

In the preceding paper,[1] we reported calculations of electron inelastic mean free paths (IMFPs) of 50–2000 eV electrons in 27 elemental solids. These calculations were based on an algorithm due to Penn,[2] which combines experimental optical data for each material (to describe the dependence of the inelastic scattering probability on energy loss) and the theoretical Lindhard dielectric function[3] (to describe the dependence of this scattering probability on momentum transfer). We fitted the calculated IMFPs to a modified form of the Bethe equation[1] for inelastic electron scattering in matter and found that the four parameters in this equation could be empirically related to several material parameters (atomic weight, density and number of valence electrons per atom). The resulting equation, referred to as TPP-2, gave IMFP values for the 27 elements which differed from those initially calculated by 13% (root mean square). The TPP-2 formula could thus be used to estimate IMFP values in other materials.

We report here IMFP calculations for 50–2000 eV electrons in 15 inorganic compounds (Al_2O_3, GaAs, GaP, InAs, InP, InSb, KCl, LiF, NaCl, PbS, PbTe, SiC, Si_3N_4, SiO_2 and ZnS); IMFP values for 200–2000 electrons in four of these compounds have been given in a previous report.[4] These 15 compounds were chosen since the needed optical data were available. As for the group of elements,[1] we found substantial differences in the shapes of the IMFP versus energy curves from compound to compound for electron energies less than 200 eV. We fitted our calculated IMFP values to the modified Bethe equation as used previously[1] to obtain convenient analytical expressions for the IMFP dependence on electron energy. Finally, we compared our IMFP results with values obtained from the formula TPP-2.

As before,[1] we are interested in providing IMFP data materials over the electron energy range of interest for AES and XPS. Although quantitative surface analyses by these techniques normally require values of electron attenuation lengths (ALs), the available data are limited and are of generally inadquate accuracy.[5,6] As a result, it is difficult to draw reliable conclusions concerning the dependences of AL on material and energy. Since we use the same algorithm in a consistent way for our IMFP calculations, we expect to obtain useful information on the dependences of IMFP on energy and material. It should then be possible to obtain the desired attenuation length dependences from Monte Carlo simulations that include IMFP data and elastic scattering information.[7]

IMFP CALCULATION

The method for calculating IMFPs has been described previously.[1,4] We use the Penn[2] algorithm, which is expected to give useful results for electron energies above 50 eV.[1] We have, in addition, calculated IMFPs for electron energies between 10 and 40 eV and display these results in the figures presented below to show the trends of IMFP versus energy more completely; these results should be considered only as rough estimates. IMFP values were calculated using Eqn. (14) of Ref. 4 for electron energies between 10 and 800 eV and Eqn. (16) of Ref. 4 was used for energies between 800

and 2000 eV. All energies are expressed with respect to the Fermi level, which, for insulators, is usually assumed to be located midway between the valence band maximum and the conduction band minimum.

For each material, we need values of the energy-loss function $Im[-1/\varepsilon(\omega)]$, where $\varepsilon(\omega)$ is the complex dielectric constant for photon energy $\hbar\omega$ (or the corresponding energy loss ΔE in an inelastic electron scattering event).[8] The dielectric constant can be expressed as

$$\varepsilon(\omega) = \varepsilon_1 + i\varepsilon_2 \tag{1a}$$

where

$$\varepsilon_1 = n^2 - k^2 \tag{1b}$$

$$\varepsilon_2 = 2nk \tag{1c}$$

n is the index of refraction and k is the extinction coefficient. We obtain n and k data for each material from the sources[9-11] or the procedures shown in Table 1 and then calculate $Im(-1/\varepsilon) = \varepsilon_2/(\varepsilon_1^2 + \varepsilon_2^2)$ from Eqns (1b) and (1c).

There are two main sources of uncertainty in the use of optical data for the IMFP calculations. First, there are gaps in the data for many of the materials, generally in the soft x-ray range. In these cases, we have used atomic photoabsorption data,[10] which usually agree well with experimental measurements for solids[12] except in the details of the structures near x-ray absorption edges and in the extended x-ray absorption fine structure (EXAFS) over energies of hundreds of electron-volts above the edges. These differences are unimportant in the IMFP calculations since an integration of the energy-loss function is made over photon energy.[4] We also make use of the Kramers–Kronig transforms[13] by which n can be calculated from k, and vice versa. In some cases, we have made interpolations based on the trends expected from Ref. 10.

As an example of our procedures, Fig. 1 shows optical data for SiC. Measured values[11] of n and k for photon energies less than 30 eV are shown, together with derived values from atomic data[10] for photon energies above 100 eV. The dashed lines show the interpolations that we have made between 30 and 100 eV.
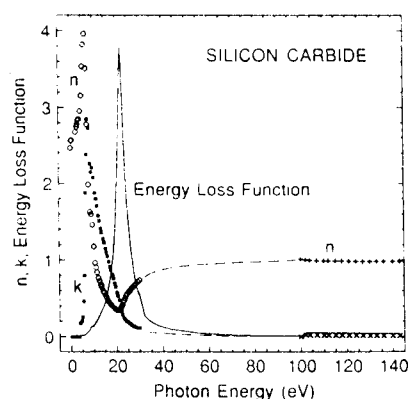

Figure 1. Plots of the optical constants n and k and the energy-loss function versus photon energy for SiC. Measured values of n (○) and k (■) from Ref. 11 are shown for photon energies of less than 30 eV; derived values of n (+) and k (×) from Ref. 10 are shown for energies of above 100 eV. The dashed lines indicate the interpolations made between 30 and 100 eV. The solid line shows the energy-loss function calculated from the optical constants.

Table 1. Sources of optical data used in the IMFP calculations

Compound	Photon energy range (eV)	Optical constants	Source of data
Al_2O_3 [a]	6–1600	n, k	Ref. 9
	1600–10 000	n, k	Ref. 10
GaAs	1.5–23	n, k	Ref. 11
	23–100	k	Ref. 11
		n	Kramers–Kronig analysis
	100–10 000	n, k	Ref. 10
GaP	0.1–16	n, k	Ref. 11
	16–100	k	Ref. 10 and 11
		n	Kramers–Kronig analysis
	100–10 000	n, k	Ref. 10
InAs	0.3–25	n, k	Ref. 11
	25–30	n, k	Interpolation
	30–100	k	Ref. 10 and interpolation
		n	Kramers–Kronig analysis
	100–10 000	n, k	Ref. 10
InP	1.3–20	n, k	Ref. 11
	20–100	k	Ref. 10 and interpolation
		n	Kramers–Kronig analysis and interpolation
	100–10 000	n, k	Ref. 10
InSb	0.1–25	n, k	Ref. 11
	25–100	k	Ref. 10 and 11
		n	Interpolation (25–40 eV) and Kramers–Kronig analysis
	100–10 000	n, k	Ref. 10
KCl	6.9–43	n, k	Ref. 11
	43–100	k	Ref. 10 and interpolation
		n	Kramers–Kronig analysis and interpolation
	100–10 000	n, k	Ref. 10
LiF	10–30	n, k	Ref. 11
	30–100	k	Ref. 11
		n	Kramers–Kronig analysis
	100–10 000	n, k	Ref. 10
NaCl	7.6–26	n, k	Ref. 11
	26–100	k	Ref. 10 and interpolation
		n	Kramers–Kronig analysis and interpolation
	100–10 000	n, k	Ref. 10
PbS	0.1–25	n, k	Ref. 11
	25–100	k	Ref. 11
		n	Kramers–Kronig analysis and interpolation
	100–10 000	n, k	Ref. 10
PbTe	0.5–17	n, k	Ref. 11
	17–100	k	Ref. 11
		n	Kramers–Kronig analysis and interpolation
	100–10 000	n, k	Ref. 10
SiC	0.2–30	n, k	Ref. 11
	30–100	k	Ref. 10 and interpolation
		n	Kramers–Kronig analysis and interpolation
	100–10 000	n, k	Ref. 10
Si_3N_4	4.5–24	n, k	Ref. 11
	24–100	k	Ref. 10 and interpolation
		n	Kramers–Kronig analysis and interpolation
	100–10 000	n, k	Ref. 10
SiO_2 [b]	0.002–2000	n, k	Ref. 11
	2000–10 000	n, k	Ref. 10
ZnS	2–100	n, k	Ref. 11
	100–10 000	n, k	Ref. 10

[a] Amorphous form.
[b] Glassy form.

There are no core levels with binding energies between 30 and 100 eV for SiC and thus no substantial structure is expected in the optical constants for the 30–100 eV photon energy range. The solid line in Fig. 1 shows the calculated energy-loss function, which has a prominent peak at ~ 22 eV and a much weaker structure near 100 eV corresponding to the onset of Si L-shell excitations.

A second source of uncertainty in the use of the optical data[9,11] is the accuracy of the tabulated data. The uncertainty for any compound will depend on the magnitudes of the optical constants, the technique by which they were measured, the spectral range and the purity and structural perfection of the compound.[11] Fortunately, the overall consistency of a data set for a material can be evaluated with the use of two useful integral equations or sum rules involving the loss function: the oscillator strength or f-sum rule and a limiting form of the Kramers–Kronig integral.[13-16] The f-sum can be evaluated as the total effective number of electrons per atom or moecule Z_{eff} contributing to the inelastic scattering

$$Z_{eff} = (2/\pi\hbar^2\Omega_p^2) \int_0^{\Delta E_{max}} \Delta E\, Im[-1/\varepsilon(\Delta E)]\, d(\Delta E) \quad (2)$$

where $\Omega_p = (4\pi n_a e^2/m)^{1/2}$, $n_a = N_a \rho/M$ is the density of atoms or molecules, N_a is Avogadro's number, ρ is the bulk density and M is the atomic or molecular weight. When the upper limit in Eqn. (2), ΔE_{max}, is equal to infinity, Z_{eff} should be equal to Z, the total number of electrons per atom or molecule.

The Kramers–Kronig (KK) relations[13,14] enable $Re[1/\varepsilon(\omega)]$ to be obtained from $Im[1/\varepsilon(\omega)]$ if the latter is known over a sufficiently wide frequency range. This relation can be simplified as follows

$$P_{eff} = (2/\pi) \int_0^{\Delta E_{max}} (1/\Delta E)$$
$$\times Im[-1/\varepsilon(\Delta E)]\, d(\Delta E) + Re[1/\varepsilon(0)] \quad (3a)$$

where $\varepsilon(0)$ is the limiting value of ε as $\omega \to 0$. For conductors, $Re[1/\varepsilon(0)]$ is zero and, in the limit $\Delta E_{max} \to \infty$, Eqn. (3a) becomes the perfect-screening sum rule that we have used previously.[4] For non-conductors, $n \gg k$ at low frequencies and Eqn. 3(a) becomes

$$P_{eff} = (2/\pi) \int_0^{\Delta E_{max}} (1/\Delta E)$$
$$\times Im[-1/\varepsilon(\Delta E)]\, d(\Delta E) + n^{-2}(0) \quad (3b)$$

where $n(0)$ is the limiting value of refractive index at frequencies below those where absorption maxima are observed. In the limit $\Delta E_{max} \to \infty$, $P_{eff} \to 1$; this integral relation will be termed the KK-sum.

Table 2 shows a listing of the errors in the f-sum and those of the KK-sum for the compounds for which we could obtain satisfactory values of $n(0)$.[11] We evaluated Eqs (2) and (3b) with $\Delta E_{max} = 10\,000$ eV and made comparisons with the values of Z_{eff} and P_{eff} expected with $\Delta E_{max} = \infty$. We were not able to obtain reliable values of $n(0)$ for three compounds and we therefore show limiting values for the KK-sum error that were obtained by assuming $n^{-2}(0)$ in Eqn. (3b) to be zero. We also chose not to estimate the contributions to Z_{eff} due to excitations with energies of $> 10^4$ eV in the indium and lead

Table 2. Errors in the f-sum (Eqn. (2)) and the KK-sum rules (Eqn. (3b)) for the indicated compounds[a]

Compound	Error in f-sum rule (%)	Error in KK-sum rule (%)
Al_2O_3	-6	-25
GaAs	-13	-37
GaP	-8	-17
InAs	>-5	-31
InP	>12	3
InSb	>-10	>-40
KCl	-1	-25
LiF	-5	-30
NaCl	-5	-32
PbS	>-13	-11
PbTe	>-12	>12
SiC	-2	-7
Si_3N_4	-8	>-34
SiO_2	-6	5
ZnS	-7	-19

[a] Both sums have been evaluated with $\Delta E_{max} = 10\,000$ eV. A minus (plus) indicates that the values of Z_{eff} and P_{eff} were less than (greater than) the expected values. We were not able to obtain reliable values of $n(0)$ for InSb, PtTe and Si_3N_4 from Ref. 11; we show limiting values of the KK-sum error for those compounds that have been obtained by assuming $n^{-2}(0)$ in Eqn. (3b) to be zero. We also show limiting values of the f-sum errors for the indium and lead compounds owing to the neglect of excitations with energies greater than 10^4 eV in the evaluation of Eqn. (2).

compounds since the f-sum errors were generally much smaller and therefore less significant than the KK-sum errors. The root mean square (RMS) error for the f-sum rule is $\sim 8\%$ while that for the KK-sum rule is $\sim 24\%$.

We note here that, in out review of the optical data for LiF and ZnS, we found differences in the 100–2000 eV range between the values listed in Ref. 11 that had been derived from Ref. 10 and those that we calculated from the same source.[17] Our values of k are twice those in Ref. 11 and led to smaller errors in the f-sum than those reported previously;[1] these errors were also decreased by an increase in the selected value of ΔE_{max}. Our IMFP results for LiF and ZnS thus supersede the values presented earlier.[1]

The errors given in Table 2 indicate likely uncertainties of the optical data. It is clear from Eqn. (2) that the f-sum integration is influenced appreciably by optical data in the 50–10 000 eV range while, from Eqn. (3b), the KK-sum integration is influenced mainly by data in the 2–50 eV range.[18] The IMFP calculation is based on an integration of $Im(-1/\varepsilon)$, for which the main contributions come from intermediate energies, roughly 5–200 eV.[18] The errors in Table 2 therefore give only an approximate guide to possible errors in the calculated IMFPs. Nevertheless, it is apparent that most of the errors in Table 2 are negative, i.e. the values of $Im(-1/\varepsilon)$ are lower than expected. While the various optical measurements giving rise to the data in Table 1 may have been performed correctly, we note that errors in

the measurements may have been introduced by the presence of surface inpurities, surface roughness or regions having lower density than the tabulated bulk values. We discuss below how the errors in Table 2 could affect our IMFP results.

The IMFP calculation requires specification of the Fermi energy for each compound.[2,4] We have chosen arbitrarily a value of $E_F = 15$ eV for the calculations reported here since variation of this parameter from 10 to 15 eV changed the calculated IMFPs by a maximum of 0.32 Å at an electron energy of 50 eV and by ~ 0.1 Å at 2000 eV.

As before,[1] we expect our IMFP calculations to be useful for electron energies greater than about 50 eV. The uncertainties in the calculated IMFPs at low energies (50–200 eV) will be greater than at higher energies, but it is not possible for us to estimate these uncertainties reliably.

IMFP RESULTS

Table 3 shows IMFP values calculated from the optical data for 50–2000 eV electrons in the 15 compounds. Plots of IMFP versus electron energy are shown in Figs 2–10 for Al_2O_3, GaAs, InAs, InP, InSb, KCl, SiC, Si_3N_4 and SiO_2 as examples of our results. These compounds were selected to illustrate the general trends and the differences in both the magnitudes of the IMFPs at a given energy and the differences in the shapes of the curves. The inset in each figure shows IMFP values at low energies (< 200 eV) on an expanded energy scale; we emphasize that, for the reasons presented earlier, the data shown for energies between 10 and 40 eV are presented to indicate trends and should be regarded only as rough estimates. As was found in our analysis of IMFP data for the group of 27 elements,[1] there are substantial variations in the shapes of the IMFP versus
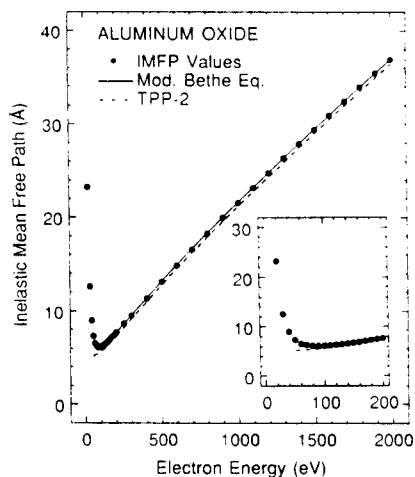

Figure 3. IMFP results for GAs as a function of electron energy; see caption to Fig. 2.

Figure 4. IMFP results for InAs as a function of electron energy; see caption to Fig. 2.

Figure 2. IMFP values (solid circles) calculated for Al_2O_3 as a function of electron energy. IMFP values are shown for 10–40 eV electrons to illustrate trends but these results are not considered to be reliable (see text). The solid line is a fit to the IMFP values with the modified Bethe equation (Eqn. (4)); values of the parameters found in the fit are given in Table 4. The dashed line shows IMFP values calculated from the predictive formula TPP-2 (Eqn. (4)) where values of the four parameters were calculated from property data for Al_2O_3 using Eqn. (5), as indicated in Table 7. The inset shows the low-energy region on an expanded energy scale.
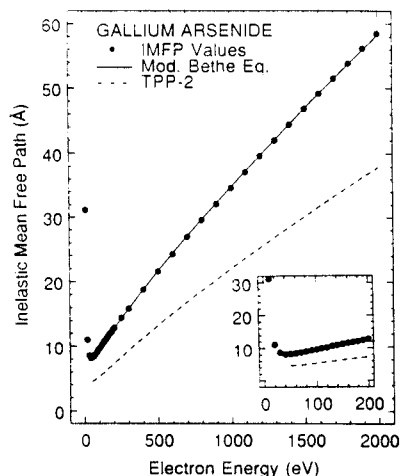

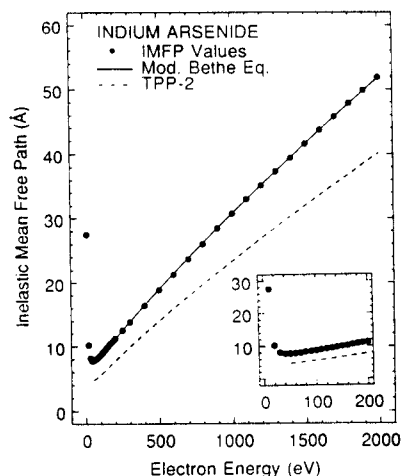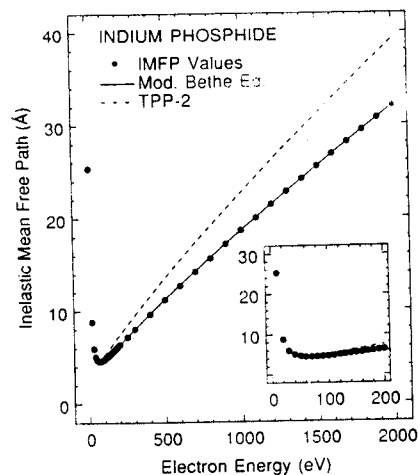**Figure 5.** IMFP results for InP as a function of electron energy; see caption to Fig. 2.

Table 3. IMFPs as a function of electron energy for 15 inorganic compounds[a]

Inelastic mean free path (Å)

Electron energy (eV)	Al₂O₃	GaAs	GaP	InAs	InP	InSb	KCl	LiF	NaCl	PbS	PbTe	SiC	Si₃N₄	SiO₂	ZnS
50	7.3	8.3	5.6	7.8	4.8	8.1	7.5	7.7	7.7	4.8	4.3	4.7	6.6	8.0	5.8
	(5.2)	(4.5)	(4.2)	(4.7)	(4.4)	(5.0)	(4.4)	(5.4)	(4.1)	(5.1)	(5.4)	(3.9)	(4.3)	(4.2)	(4.3)
100	6.2	9.7	6.5	8.8	4.9	9.5	7.8	6.8	8.8	5.6	5.5	4.9	6.4	7.7	6.5
	(5.6)	(5.3)	(5.0)	(5.6)	(5.3)	(5.9)	(5.9)	(6.1)	(5.4)	(5.5)	(5.9)	(4.6)	(4.9)	(5.2)	(4.8)
150	6.8	11.3	7.8	10.0	5.6	10.9	9.3	7.6	10.5	6.7	6.6	5.8	7.3	8.8	7.7
	(6.4)	(6.3)	(6.0)	(6.6)	(6.4)	(7.1)	(7.3)	(7.0)	(6.6)	(6.4)	(6.9)	(5.4)	(5.7)	(6.1)	(5.6)
200	7.7	12.9	9.0	11.3	6.4	12.3	10.9	8.6	12.2	7.8	7.7	6.8	8.4	10.0	8.9
	(7.3)	(7.3)	(7.0)	(7.8)	(7.5)	(8.3)	(8.7)	(8.0)	(7.8)	(7.3)	(8.0)	(6.3)	(6.6)	(7.2)	(6.4)
300	9.6	15.9	11.4	13.9	8.1	15.2	14.2	10.7	15.6	10.0	9.8	8.7	10.7	12.6	11.3
	(9.2)	(9.4)	(9.0)	(9.9)	(9.6)	(10.6)	(11.3)	(10.1)	(10.1)	(9.3)	(10.1)	(8.0)	(8.4)	(9.2)	(8.1)
400	11.4	18.8	13.7	16.4	9.7	18.1	17.3	12.8	18.8	12.1	11.9	10.5	12.7	15.2	13.6
	(11.0)	(11.3)	(10.9)	(12.0)	(11.6)	(12.8)	(13.9)	(12.1)	(12.3)	(11.2)	(12.1)	(9.7)	(10.1)	(11.1)	(9.8)
500	13.2	21.6	16.0	18.9	11.2	20.9	20.3	14.9	21.9	14.1	13.9	12.2	14.7	17.6	15.8
	(12.8)	(13.2)	(12.8)	(14.0)	(13.6)	(15.0)	(16.3)	(14.1)	(14.5)	(13.0)	(14.1)	(11.3)	(11.8)	(13.0)	(11.4)
600	14.9	24.3	18.1	21.3	12.8	23.7	23.2	16.9	24.9	16.1	15.8	13.9	16.6	20.0	17.9
	(14.5)	(15.1)	(14.6)	(16.0)	(15.5)	(17.1)	(18.7)	(16.1)	(16.6)	(14.8)	(16.1)	(12.9)	(13.4)	(14.9)	(13.0)
700	16.6	27.0	20.2	23.7	14.2	26.4	26.0	18.9	27.8	18.0	17.7	15.5	18.5	22.4	20.0
	(16.2)	(16.9)	(16.3)	(17.9)	(17.3)	(19.1)	(21.1)	(18.0)	(18.6)	(16.5)	(17.9)	(14.5)	(15.0)	(16.7)	(14.5)
800	18.3	29.6	22.3	26.0	15.7	29.0	28.7	20.8	30.7	19.8	19.6	17.1	20.4	24.7	22.0
	(17.9)	(18.6)	(18.1)	(19.7)	(19.1)	(21.1)	(23.3)	(19.9)	(20.6)	(18.2)	(19.8)	(16.0)	(16.5)	(18.5)	(16.1)
900	20.0	32.1	24.3	28.4	17.2	31.8	31.4	22.8	33.5	21.8	21.6	18.7	22.3	27.0	24.0
	(19.5)	(20.3)	(19.7)	(21.6)	(20.9)	(23.1)	(25.6)	(21.8)	(22.6)	(19.8)	(21.6)	(17.5)	(18.1)	(20.2)	(17.5)
1000	21.6	34.7	26.3	30.7	18.7	34.4	34.0	24.6	36.2	23.6	23.4	20.3	24.1	29.3	26.0
	(21.2)	(22.0)	(21.4)	(23.4)	(22.7)	(25.0)	(27.8)	(23.6)	(24.5)	(21.5)	(23.4)	(19.0)	(19.6)	(21.9)	(19.0)
1100	23.2	37.1	28.3	33.0	20.1	37.0	36.6	26.5	39.0	25.4	25.1	21.8	25.9	31.5	27.9
	(22.8)	(23.7)	(23.0)	(25.1)	(24.4)	(26.9)	(29.9)	(25.4)	(26.4)	(23.1)	(25.1)	(20.4)	(21.1)	(23.6)	(20.4)
1200	24.8	39.6	30.2	35.2	21.4	39.5	39.2	28.4	41.7	27.1	26.9	23.3	27.7	33.7	29.8
	(24.3)	(25.3)	(24.6)	(26.9)	(26.1)	(28.8)	(32.1)	(27.2)	(28.3)	(24.6)	(26.8)	(21.9)	(22.6)	(25.3)	(21.9)
1300	26.4	42.0	32.2	37.3	22.8	42.0	41.7	30.2	44.4	28.9	28.6	24.8	29.4	35.8	31.7
	(25.9)	(27.0)	(26.2)	(28.6)	(27.8)	(30.6)	(34.2)	(28.9)	(30.2)	(26.2)	(28.5)	(23.3)	(24.0)	(27.0)	(23.3)
1400	27.9	44.4	34.1	39.5	24.2	44.4	44.2	32.0	47.0	30.6	30.3	26.3	31.1	38.0	33.6
	(27.4)	(28.6)	(27.8)	(30.3)	(29.4)	(32.4)	(36.3)	(30.6)	(32.0)	(27.7)	(30.2)	(24.7)	(25.4)	(28.6)	(24.6)
1500	29.5	46.8	36.0	41.6	25.5	46.8	46.7	33.8	49.6	32.3	32.0	27.8	32.9	40.1	35.4
	(29.0)	(30.2)	(29.4)	(32.0)	(31.1)	(34.2)	(38.3)	(32.4)	(33.8)	(29.3)	(31.8)	(26.1)	(26.9)	(30.2)	(26.0)
1600	31.0	49.2	37.8	43.7	26.8	49.2	49.1	35.6	52.2	33.9	33.7	29.2	34.6	42.2	37.3
	(30.5)	(31.7)	(30.9)	(33.6)	(32.7)	(36.0)	(40.4)	(34.1)	(35.6)	(30.8)	(33.5)	(27.4)	(28.3)	(31.8)	(27.4)
1700	32.5	51.6	39.7	45.8	28.1	51.6	51.6	37.3	54.8	35.6	35.3	30.7	36.3	44.3	39.1
	(32.0)	(33.3)	(32.4)	(35.3)	(34.3)	(37.8)	(42.4)	(35.8)	(37.4)	(32.3)	(35.1)	(28.8)	(29.7)	(33.4)	(28.7)
1800	34.0	53.9	41.5	47.9	29.4	53.9	54.0	39.1	57.4	37.2	37.0	32.1	37.9	46.4	40.9
	(33.5)	(34.8)	(33.9)	(36.9)	(35.9)	(39.5)	(44.4)	(37.4)	(39.2)	(33.8)	(36.7)	(30.1)	(31.1)	(35.0)	(30.1)
1900	35.5	56.2	43.4	49.9	30.7	56.2	56.4	40.8	59.9	38.9	38.6	33.5	39.6	48.4	42.7
	(34.9)	(36.4)	(35.5)	(38.6)	(37.5)	(41.3)	(46.4)	(39.1)	(40.9)	(35.2)	(38.3)	(31.5)	(32.4)	(36.5)	(31.4)
2000	36.9	58.5	45.2	52.0	32.0	58.5	58.8	42.5	62.4	40.5	40.2	35.0	41.3	50.5	44.5
	(36.4)	(37.9)	(36.9)	(40.2)	(39.1)	(43.0)	(48.4)	(40.7)	(42.7)	(36.7)	(39.9)	(32.8)	(33.8)	(38.1)	(32.7)

[a] The values on the first line for each energy are IMFPs calculated from optical data while the values in parentheses on the second line are IMFPs calculated from TPP-2 (Eqns (4) and (5)).
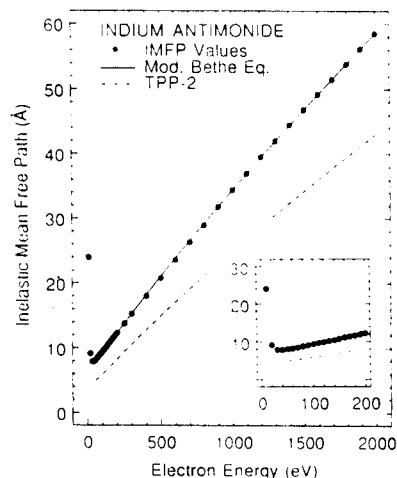
Figure 6. IMFP results for InSb as a function of electron energy;
see caption to Fig. 2.

Figure 9. IMFP results for Si_3N_4 as a function of electron energy;
see caption to Fig. 2.

energy curves in the 50–200 eV range for this group of
compounds.

We have analyzed the compound IMFP data as we
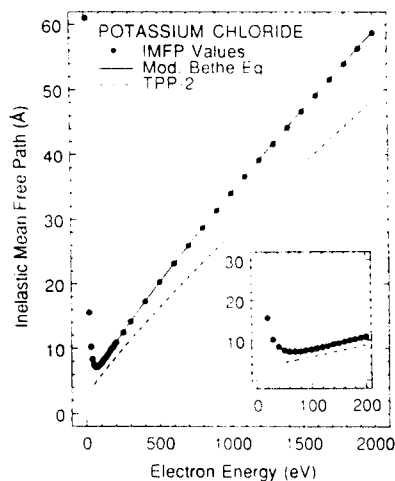did for the elements.[1] We fitted IMFP values for each

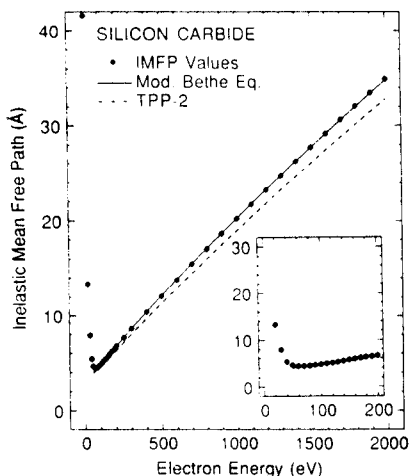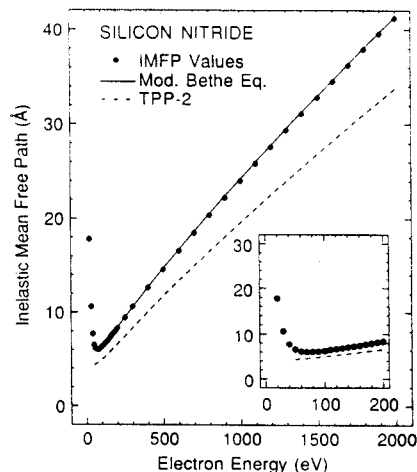**Figure 7.** IMFP results for KCl as a function of electron energy;
see caption to Fig. 2.

material to a modified form of the Bethe equation[19] for
inelastic electron scattering in matter; the modifications
were made as suggested by Inokuti[20] and Ashley[21] to
describe adequately the IMFP dependence on energy
over the 50–2000 eV range.

The modified Bethe equation is

$$\lambda = E/\{E_p{}^2[\beta \ln(\gamma E) - (C/E) + (D/E^2)]\} \qquad (4)$$

where λ is the IMFP (in Å), E is the electron energy (in
eV), $E_p = 28.8 (N_v\rho/M)^{1/2}$ is the free-electron plasmon
energy (in eV), ρ is the density (in g cm^{-3}), N_v is the
number of valence electrons per atom (for elements) or
molecule (for compounds) and M is the atomic or
molecular weight; β, γ, C and D are parameters. The
last two terms in Eqn. (4) enable the effects of electron
exchange and other departures from the first Born
approximation at low energies to be included in an
empirical manner.

The solid lines in Figs 2–10 show fits of Eqn. (4) to
our IMFP data (Table 3) over the 50–2000 eV range.
Values of the parameters β, γ, C and D for each material
are listed in Table 4, and values of the material param-
eters used in our analysis are shown in Table 5.

Figure 8. IMFP results for SiC as a function of electron energy;
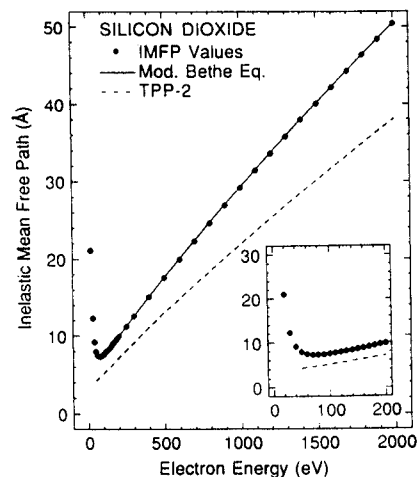see caption to Fig. 2.

Figure 10. IMFP results for SiO_2 as a function of electron energy;
see caption to Fig. 2.

Table 4. Values of the parameters β, γ, C and D found in the fits of Eqn. (4) to the IMFP data for each compound, together with values of β_{opt} calculated from Eqn. (6)

Compound	β_{opt} (eV^{-1} Å^{-1})	β (eV^{-1} Å^{-1})	γ (eV^{-1})	C (Å^{-1})	D (eV Å^{-1})
Al$_2$O$_3$	0.0131	0.0142	0.0714	0.977	26.1
GaAs	0.0274	0.0332	0.0353	0.304	32.2
GaP	0.0297	0.0340	0.0614	0.855	31.4
InAs	0.0379	0.0431	0.0467	1.70	77.4
InP	0.0526	0.0565	0.0830	3.60	102.5
InSb	0.0408	0.0440	0.0623	2.61	104.4
KCl	0.0338	0.0368	0.0956	1.08	6.24
LiF	0.0127	0.0133	0.0980	1.15	29.2
NaCl	0.0233	0.0263	0.0725	0.859	24.5
PbS	0.0345	0.0372	0.0792	1.31	38.3
PbTe	0.0446	0.0474	0.0916	2.26	79.0
SiC	0.0192	0.0217	0.0743	0.607	10.3
Si$_3$N$_4$	0.0137	0.0156	0.0610	0.540	13.0
SiO$_2$	0.0149	0.0158	0.0925	1.10	27.1
ZnS	0.0130	0.0149	0.0592	0.332	10.4

In our investigations of the IMFP results for the group of 27 elements,[1] we found that the four parameters in Eqn. (4) could be related empirically to other material properties data, as follows

$$\beta = -0.0216 + 0.944/(E_p^2 + E_g^2)^{1/2}$$
$$+ 7.39 \times 10^{-4}\rho \tag{5a}$$

$$\gamma = 0.191\rho^{-0.50} \tag{5b}$$

$$C = 1.97 - 0.91U \tag{5c}$$

$$D = 53.4 - 20.8U \tag{5d}$$

$$U = N_v\rho/M \tag{5e}$$

where E_g is the band-gap energy (in eV) for non-conductors. Equations (4) and (5) constitute our formula TPP-2 for predicting IMFPs in other materials. We now assess how IMFP predictions of the formula TPP-2 compare with the values calculated for each compound (Table 3) and how values of the four parameters in Eqn. (4) obtained in the fits to the IMFP values

Table 5. Values of material parameters used in the analysis of the IMFP data for the indicated compounds

Compound	ρ (g cm^{-3})	N_v	E_p (eV)	E_g (eV)
Al$_2$O$_3$	3.97	24	27.8	9.0
GaAs	5.31	8	15.6	1.35
GaP	4.13	8	16.5	2.24
InAs	5.67	8	14.1	0.36
InP	4.79	8	14.8	1.27
InSb	5.78	8	12.7	0.17
KCl	1.98	8	13.3	7.4
LiF	2.64	8	26.0	11.8
NaCl	2.17	8	15.7	7.42
PbS	7.59	10	16.2	0.37
PbTe	8.16	10	14.2	0.25
SiC	3.21	8	23.0	2.3
Si$_3$N$_4$	3.44	32	25.5	5.25
SiO$_2$	2.19	16	22.0	9.1
ZnS	4.08	18	25.2	3.6

for each compound (Table 4) compare to those predicted by Eqn. (5).

The dashed lines in Figs 2–10 show IMFP values for each compound predicted by TPP-2 (Eqns (4) and (5)). For all compounds except InP, PbS and PbTe, the IMFPs calculated from TPP-2 were lower at all energies than those directly calculated (Table 3). Even for these three compounds, there were some energies for which the IMFPs from TPP-2 were less than the calculated values. A more quantitative comparison is presented in Table 6, from which it can be seen that the largest differences frequently occurred at the lowest energy considered (50 eV) and some at the highest energy (2000 eV). The largest negative percentage difference is for SiO$_2$ (47% at 50 eV) and the largest positive percentage difference is for PbTe (26% at 50 eV). An overall comparison is made using values for the RMS differences listed in the final column of Table 6; such a comparison is believed useful even though the differences are systematic rather than random. The largest RMS difference is for GaAs (−41%) and the average RMS difference is ~23%. This value for the RMS difference is almost double the corresponding value found for the group of 27 elements (13%),[1] and will be discussed further below.

Figure 11 shows a plot of the values of β (solid circles) determined from our least-squares fits for each compound (Table 4) versus $(E_p^2 + E_g^2)^{-1/2}$. This figure also includes values of β determined from similar fits for our group of 27 elements.[1] The dashed and solid lines in Fig. 11 show the dependence expected fom Eqn. 5(a) with $\rho = 0$ and $\rho = 10$ g cm^{-3}, respectively. As a group, the compounds in Fig. 11 generally have lower values of β than the group of elements. This result is not surprising since many of the compounds have lower densities than the elements considered previously.

Table 6. Values of the largest negative percentage difference, the largest positive percentage difference and the root-mean-square (RMS) percentage difference found for each compound in comparisons of the IMFP results from TPP-2 (Eqns (4) and (5)) and those shown in Table 3[a]

Compound	Largest positive difference	E_{pos} (eV)	Largest negative difference (%)	E_{neg} (eV)	RMS diff. (%)
Al$_2$O$_3$	—	—	−30	50	−8
GaAs	—	—	−46	50	−41
GaP	—	—	−25	50	−21
InAs	—	—	−39	50	−30
InP	22	2000	−7	50	17
InSb	—	—	−39	60	−32
KCl	—	—	−41	50	−22
LiF	—	—	−30	50	−9
NaCl	—	—	−47	50	−36
PbS	6	50	−9	2000	−7
PbTe	26	50	−1	2000	7
SiC	—	—	−17	50	−7
Si$_3$N$_4$	—	—	−35	50	−21
SiO$_2$	—	—	−47	50	−29
ZnS	—	—	−28	300	−27

[a] The sign of the difference indicates whether the values from TPP-2 are systematically lower (−) or higher (+) than the values of Table 3. E_{pos} and E_{neg} are the energies at which the largest positive and negative differences, respectively, occur.
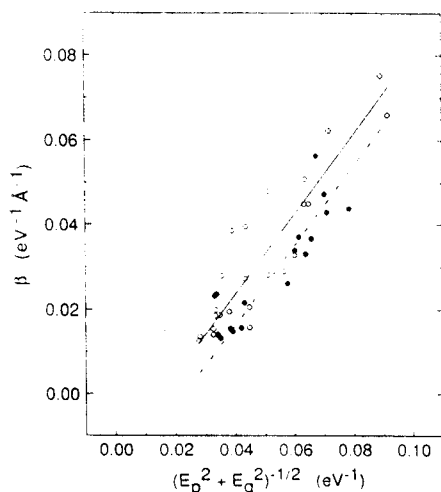
S. TANUMA, C. J. POWELL AND D. R. PENN

Figure 11. Values of β (solid circles) found for each compound (Table 4) from the fits of Eqn. (4) to the IMFPs calculated from optical data (Table 3) plotted versus $(E_p^2 + E_g^2)^{-1/2}$ (Table 5). The open circles show the corresponding values for our group of 27 elements (Ref. 1). The dashed line is a plot of $[0.944 \, (E_p^2 + E_g^2)^{-1/2} - 0.0216]$ while the solid line shows a plot of Eqn. (5a) for $\rho = 10$ g cm^{-3}.

We were guided in the development of Eqn. 5(a) by previous IMFP calculations[22,23] in which a parameter $\bar{E}$ was introduced to represent the centroid of the energy-loss function. In their analyses of data for a group of elements and inorganic compounds, Szajman and Leckey[22] found that $\bar{E}$ was approximately equal to $(E_p + E_g)$. We previously[4] developed a predictive IMFP formula for the 200–2000 eV energy range and found that there were better fits (i.e. there was less scatter) when β was expressed as a function of $(E_p^2 + E_g^2)^{-1/2}$, although at that time there was only a small number of non-conductors among the group of materials. It is therefore appropriate to examine here whether the inclusion of E_g in Eqn. 5(a) is warranted. Figure 12 shows a plot of β versus E_p^{-1} and it can be seen that the scatter of points is greater than in Fig. 11. A plot of β versus $(E_p + E_g)^{-1}$, not shown here, gave slightly more
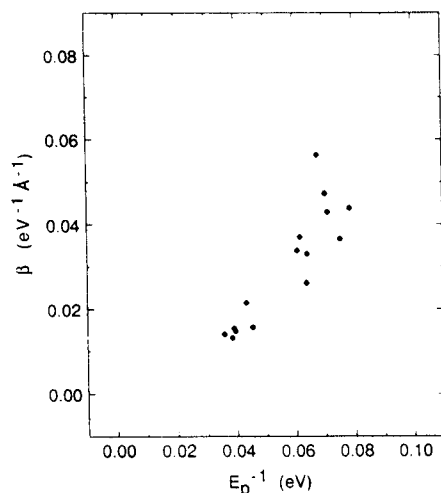
scatter than that found in Fig. 11. We conclude that inclusion of E_g in Eqn. (5a) is worthwhile and that the dependence of β on E_g in Eqn. (5a) is the best of the three options that we considered.

Figure 13 shows values of γ (solid circles) for each compound (Table 4) plotted against density; the corresponding values for our group of elements are shown as open circles together with Eqn. (5b).[1] Most of the γ values for the compounds lie below the solid line representing Eqn. (5b), although the scatter of points about the line is only a little greater than for the group of elements.

Figure 14 and 15 show plots of the values of C and D for each compound (Table 4) together with Eqns 5(c) and 5(d), respectively, versus U (Eqn. 5(e)). The data for the compounds are shown as solid circles and the corre-
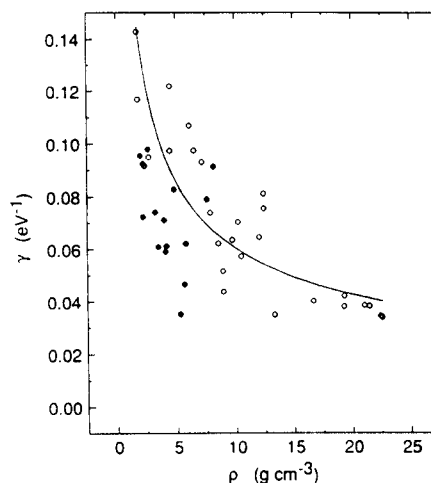

Figure 13. Values of γ (solid circles) found for each compound (Table 4) found from the fits of Eqn. (4) to the calculated IMFPs (Table 3) plotted versus density. The open circles show the corresponding results for our group of elements (Ref. 1). The solid line is a plot of Eqn. 5(b).
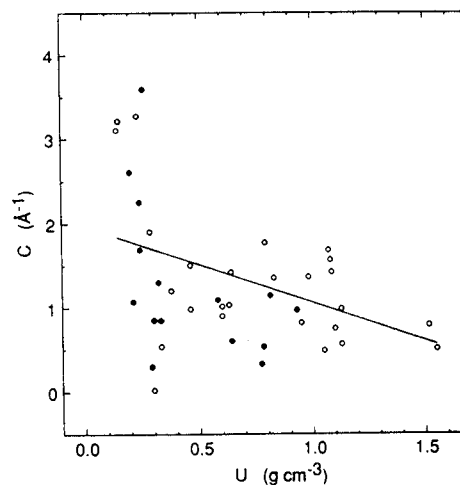

Figure 12. Values of β found for each compound (Table 4) plotted versus E_p^{-1} (Table 5).

Figure 14. Values of C (solid circles) found for each compound (Table 4) plotted versus U (Eqn. 5(e)). The open circles show the corresponding results for our group of 27 elements (Ref. 1). The solid line is a plot of Eqn. 5(c).
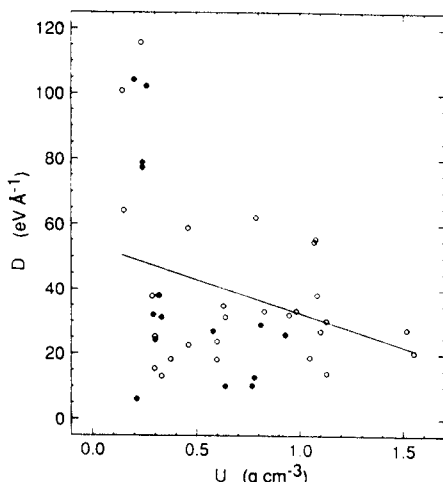
Figure 15. Values of D (solid circles) found for each compound (Table 4) plotted versus U (Eqn. 5(e)). The open circles show the corresponding results for our group of 27 elements (Ref. 1). The solid line is a plot of Eqn. 5(d).

sponding results for our group of elements are shown as open circles.[1] As we found for the elements,[1] there is more scatter in these plots at low values of U. We attribute this scatter, as before, to correlations in the values of C and D derived from the least-squares fits and to detailed differences in the shapes of the energy-loss functions for each material, which affect the shapes of the IMFP versus energy curves, particularly below 200 eV, and thus the values of C and D. Nevertheless, most of the points for the compounds in Figs 14 and 15 lie below the lines representing Eqns 5(c) and 5(d).

A useful check in our analysis is to determine values of β valid for 'high' electron energies. Such values, designated β_{opt}, can be obtained from the following relations[4]

$$\beta_{opt} = M_{tot}^2/28.8N_v \quad (\text{eV}^{-1}\text{Å}^{-1}) \qquad (6a)$$

where

$$M_{tot}^2 = \int_0^\infty \frac{2R \, Im[1/\varepsilon(\Delta E)] \, d(\Delta E)}{\pi h^2 \Omega_p^2} \qquad (6b)$$

M_{tot}^2 is the square of the dipole matrix element for all possible inelastic scattering processes and R is the Rydberg energy (13.606 eV). Table 4 shows values of β_{opt} calculated from Eqn. (6b), where the upper limit of the integral has been chosen to be 10000 eV. These values of β_{opt} represent the slopes of Fano plots (in which E/λ is plotted versus ln E) in the so-called asymptotic Bethe region.[24] The values of β in Table 4 exceed those of β_{opt} by amounts varying from 5 to 21%, with an RMS difference of 12%. It is expected[24] that the slopes of the Fano plots for the 50–2000 eV range (given by β) should exceed the asymptotic slopes β_{opt}; for this reason, Eqns (4) and (5) should not be extrapolated to higher energies.

DISCUSSION

IMFP predictive formula TPP-2

As before,[1] we have compared the IMFP values for our group of 15 compounds with values calculated from the

IMFP predictive formula TPP-2 (Eqns (4) and (5)). It is apparent from Figs 2–10 and the information in Table 6 that the TPP-2 values are generally lower than those calculated here (Table 3). Similarly, the values of β and γ derived from our fits of Eqn. (4) to the calculated IMFPs, as shown in Figs 11 and 13, are lower than expected from TPP-2.

These apparent discrepancies can be largely attributed to inadequacies of the optical data used for the IMFP calculations. Table 2 indicates that the errors in the evaluations of the f-sum and KK-sum (Eqns (2) and (3b)) for our compounds were largely negative, from which we concluded earlier that the optical values of $Im[-1/\varepsilon(\omega)]$ were systematically lower than expected. As a result, the IMFPs calculated from the optical data (Table 3) are higher than the values that would have been obtained if the sum rules had been better satisfied. Figure 16 shows a plot of the RMS errors in the comparison of our IMFP results with those expected from TPP-2 (final column of Table 6) versus the estimated average errors of the optical data. We estimated the likely errors of the optical data by simply averaging the errors in the f-sum rule and the KK-sum for each compound (Table 2). As explained earlier, these tests of the optical values of the energy-loss function emphasize regions of ΔE that are higher and lower, respectively, than those most important for the IMFP calculation, and we believe that the average error in those two sum rules is a reasonable (but approximate) indicator of the likely accuracy of the optical values of $Im[-1/\varepsilon(\omega)]$. The f-sum does, however, include significant contributions from core-electron excitations of medium- and high-Z atoms if the limit ΔE_{max} in Eqn. (2) was made appreciably greater than our chosen value of 10^4 eV.[18] Nevertheless, since the errors in the f-sum are generally small, any errors in our determination of the f-sum associated with high-energy core excitations should have little effect on the optical values of the energy-loss function that are important for our IMFP calculation.
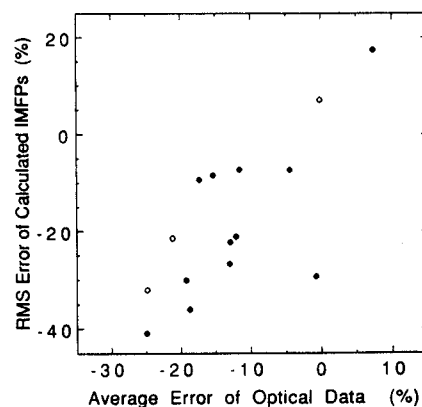

Figure 16. Plot of the RMS errors in the comparison of our IMFP values with those expected from TPP-2 for each compound (final column of Table 6) versus the average of the errors in the f-sum and KK-sum (Table 2). Points for InSb, PbTe and Si$_3$N$_4$ are shown as open circles; for these compounds, the KK-sum errors are known only as lower limits and thus the negative average optical errors are overestimated. Points for the other compounds are shown as solid circles.

Figure 16 shows an approximately linear relationship between the RMS errors in the comparison of our calculated IMFP values with those expected from TPP-2 and the estimated errors of the optical data. We also find similar correlations in plots (not shown) of the differences in the values of β and γ obtained from the IMFP calculations (Table 4) and from Eqn. (5) (Table 7) versus the estimated errors of the optical data. The correlation in Fig. 16 is striking, the scatter being no worse than expected from the RMS deviation of 13% found in the comparison of calculated IMFPs for the group of 27 elements and the values predicted by TPP-2.[1] We conclude that the IMFPs predicted by TPP-2 for the present group of inorganic compunds are likely to be more reliable than those calculated from optical data.

In principle, the optical data for each compound could be checked with the various optical sum rules and, where necessary, adjustments could be made so that the sum rules could be better satisfied: the optical constants for aluminium have been adjusted in this way.[25] We have chosen not to do this, in part because of the effort involved and in part because of the possibility that some arbitrariness might be involved. Instead, we recommend that IMFPs calculated from TPP-2 be used instead of the values calculated from optical data. We list in Table 7 values of the four parameters in TPP-2 calculated from Eqn. (5) for each compound and we show IMFPs calculated from TPP-2 in parentheses in Table 3. We also point out that the RMS error in the use of TPP-2 for calculating IMFPs of the group of elements was 13%.[1] This uncertainty is comparable to the scatter of points in Fig. 16 about the correlation line and is thus expected to be a reasonable indication of the uncertainty in using TPP-2 for predicting relative IMFPs of inorganic compounds. We also refer the reader to the previous paper[1] for a discussion of factors influencing the accuracy of IMFPs calculated from TPP-2.

IMFPs can be calculated for a given compound and electron energy from TPP-2 using appropriate values of bulk density[26] and of bandgap energy.[26,27] If values of the bandgap energy are not available for the material of

interest, it is suggested that E_g be set equal to some representative value in the range 1–3 eV for semiconductors and in the range 5–10 eV for insulators, since the magnitude of this parameter does not appreciably affect the resulting IMFP.[1] The number of valence electrons per molecule N_v is determined by counting the total number of electrons with binding energies less than about 15 eV, as indicated by the examples of Table 5. Values of E_p and U can then be computed and thus the IMFP values from Eqs (4) and (5). Our previous paper[1] gives examples of the sensitivity of IMFPs calculated from TPP-2 to the choice of parameters.

Comparisons of IMFP values with other results

Two groups have calculated IMFPs using information for $Im(-1/\varepsilon)$ from optical data or inelastic electron scattering experiments, although with differences in technical approach. Szajman and Leckey[22] report IMFP values for SiO_2 and NaCl which differ from our calculated IMFPs (Table 3) by -21% and 11%, respectively, for energies between 1000 and 2000 eV; at 200 eV, however, the Szajman and Leckey IMFP for SiO_2 is less than our value by 36%. Ashley and Anderson[28] present IMFP results for SiO_2 which differ from our values by $<9\%$ over the 100–2000 eV range; the IMFPs of Ashley and Tung[29] for Al_2O_3 are lower than our results by $\sim18\%$. The degree of consistency among these results is considered reasonable, given the differences of approach and data used in the various analyses. For comparisons made with IMFPs calculated from TPP-2, as just recommended (Table 3), the agreement with the data of Szajman and Leckey[22] is better for SiO_2 and worse for NaCl. We also find worse agreement with the SiO_2 results of Ashley and Anderson[28] and slightly better agreement with the Al_2O_3 data of Ashley and Tung.[29]

Reich et al.[30] have calculated IMFPs with an atomic model. Although this model does not adequately represent inelastic scattering processes in solids, it is expected to yield results in semi-quantitative agreement with direct calculations for solids.[1] Their IMFPs for SiO_2 are 44% lower than our IMFPs calculated from optical data at 200 eV but the difference decreases to 13% at 2000 eV. For Al_2O_3, their IMFPs are lower than our results by 40–50% over the 200–2000 eV range.

Meaningful comparisons of our IMFP results with measurements of electron attenuation lengths (ALs) are difficult because, in part, IMFPs are expected to exceed ALs on account of elastic electron scattering[7] and, in part, AL measurements may have uncertainties of up to a factor of ~2 owing to many possible systematic errors.[5,6] Nevertheless, we summarize in Fig. 17 the AL measurements for SiO_2 at two electron energies, 1150 and 1380 eV, that correspond to photoemission from the Si L_{23} shell by Mg and Al $K\alpha$ x-rays, respectively. SiO_2 is one of the relatively few materials for which multiple AL measurements have been made in different laboratories.[31–39]

Figure 17, in fact, shows greater consistency among the AL measurements than a similar plot for Si.[6] The SiO_2 plot does indicate, in addition, that the ratios of AL measurements at the two electron energies differ

Table 7. Values of the parameters β, γ, C and D calculated from Eqn. (5) for use in TPP-2 (Eqn. (4))

| Compound	β (eV^{-1} Å^{-1})	γ (eV^{-1})	C (Å^{-1})	D (eV Å^{-1})
Al_2O_3	0.0136	0.0959	1.12	34.0
GaAs	0.0426	0.0829	1.70	47.3
GaP	0.0382	0.0940	1.67	46.6
InAs	0.0496	0.0802	1.75	48.4
InP	0.0456	0.0873	1.73	47.9
InSb	0.0568	0.0794	1.79	49.3
KCl	0.0420	0.136	1.78	49.0
LiF	0.0134	0.118	1.23	36.5
NaCl	0.0344	0.130	1.70	47.2
PbS	0.0422	0.0693	1.68	46.8
PbTe	0.0508	0.0669	1.75	48.3
SiC	0.0215	0.107	1.39	40.1
Si_3N_4	0.0172	0.103	1.26	37.1
SiO_2	0.0197	0.129	1.44	41.3
ZnS	0.0184	0.0946	1.27	37.4
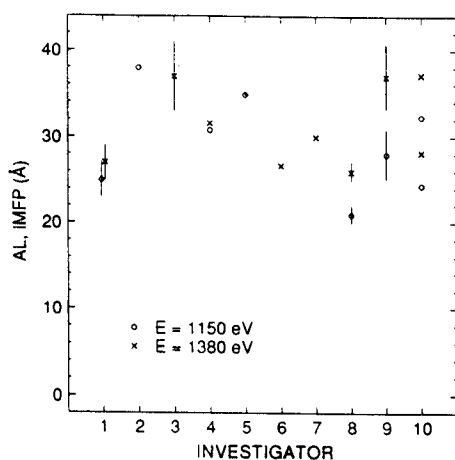
Figure 17. Plot of reported measurements of electron attenuation lengths (ALs) in SiO_2 by nine investigators (Refs 31–39) at two electron energies, 1150 and 1380 eV, corresponding to photoemission of Si L_{23}-shell electrons by Mg and Al $K\alpha$ x-rays. The values shown as investigator 10 are the IMFP results of this work. Two pairs of IMFP results are shown, one pair (with larger IMFPs) calculated from Eqn. (4) and the parameters of Table 4 and the other pair (with smaller IMFPs) calculated from TPP-2 (Eqns (4) and (5) with parameters listed in Table 7).

Figure 18. Plot of the electron energy-loss function [$Im(-1/\varepsilon(w))$] for Al_2O_3 as a function of energy loss $\hbar w$, as calculated from optical data (Table 1).

considerably, even though relative measurements would be expected to be more reliable than absolute measurements. Investigators 1 and 4 find essentially the same values for the ALs at the two energies, whereas investigators 8 and 9 find ratios of 1.24 and 1.32, respectively.

Our IMFP results for SiO_2 are shown in Fig. 17 as data for investigator 10. We show two pairs of IMFP values, the pair with larger IMFPs being calculated from Eqn. (4) and the parameter values in Table 4; these values correspond to the IMFPs calculated from the optical data in Table 3. The pair of values with smaller IMFPs in Fig. 17 were calculated from TPP-2, i.e. Eqn. (4) with parameter values calculated from Eqn. (5), as given in Table 7. The ratios of IMFPs at the two energies is 1.15 (for both pairs of IMFP data), a result consistent with the ratios reported by investigators 8 and 9 (within the reported experimental uncertainties). The recommended IMFP values (calculated by TPP-2) are slightly greater in absolute magnitude, as expected,[7] than the recent AL measurements of investigator 8.[38]

Shapes of the IMFP versus energy curves

The shapes of the IMFP versus energy curves for energies below 200 eV vary from compound to compound (Figs 2–10). For example, the calculated IMFPs for GaAs (Fig. 3) and InSb (Fig. 6) fall rapidly with increasing energy to minima near 40 eV and then increase approximately linearly to 200 eV. In contrast, the calculated IMFPs for Al_2O_3 (Fig. 2), KCl (Fig. 7) and SiO_2 (Fig. 10) decrease more gradually with increasing energy to broad minima around 70–80 eV and then slowly increase again.

The differences in the shapes of the IMFP versus energy curves are attributed, as before,[1] to differences in the shapes of the energy-loss functions [$Im(-1/\varepsilon)$] for each material. We show the energy-loss functions for Al_2O_3, GaAs and KCl in Figs 18–20 to illustrate the
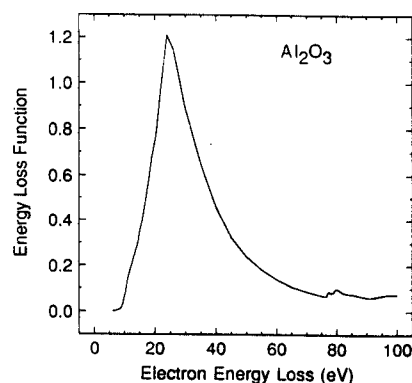
differences in the inelastic electron scattering characteristics of these materials. At low electron energies (50–200 eV), these differences in the inelastic scattering properties lead to significant differences in the shapes of the IMFP versus energy curves.

The energy at which the IMFP is a minimum is important in photoemission and related experiments
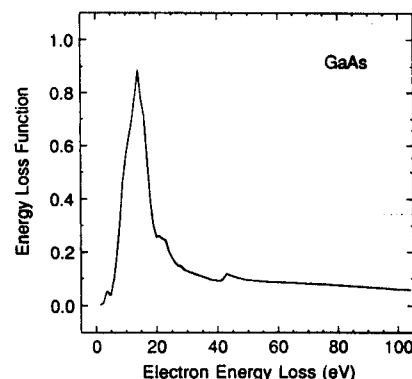

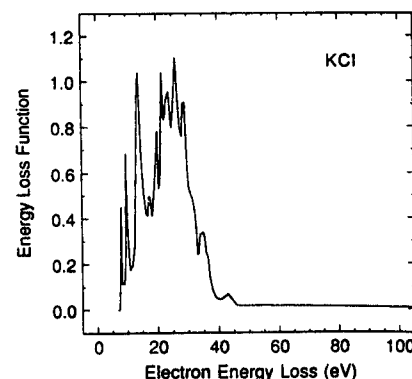**Figure 19.** Plot of the electron energy-loss function for GaAs; see caption to Fig. 18.

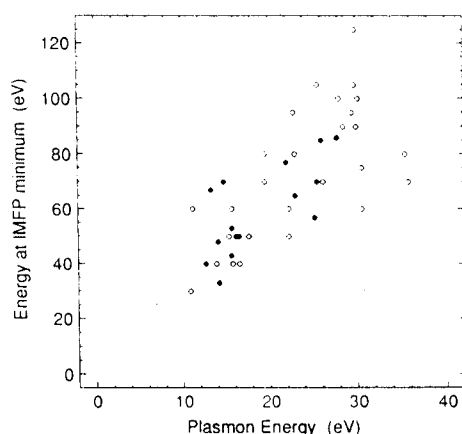**Figure 20.** Plot of the electron energy-loss function for KCl, see caption to Fig. 18.

Figure 21. Plot of the electron energy for which the IMFP calculated from optical data (Table 3) is a minimum (solid circles) versus the free-electron plasmon energy (Table 5) for the group of 15 compounds. The open circles show similar results for the group of 27 elements (Ref. 1).

with synchrotron radiation in which the photon energy is varied to obtain maximum surface sensitivity. Figure 21 is a plot of the energy for the minimum IMFP versus free-electron plasmon energy for each compound (Table 5), together with similar data for our group of elements.[1] The data for the compounds in Fig. 21 show a similar, approximately linear, dependence on plasmon energy to that found for the elements. Such a dependence is expected from free-electron theory.[40] Although the trend in Fig. 21 is reasonable, many of the elements and compounds are not free-electron-like materials and the scatter in Fig. 21 is believed to be largely due to the energy-loss functions having distributions more complex than those for plasmon excitation (as indicated, for example, in Fig. 20).

A number of so-called universal curves have been proposed for describing the dependence of IMFP or AI on electron energy.[5] Not surprisingly, the relatively

simple expressions developed in the past do not adequately represent the different shapes of IMFP versus energy curves, particularly at energies below 200 eV. Although our TPP-2 formula does give changes in the IMFP versus energy dependences at low energies that are similar to those found in the IMFP calculations (Figs 2–10), the deviations between the TPP-2 values and the calculated IMFPs become greater at 50 eV for many of the compounds (Table 6). It is not surprising, owing to substantial differences in the shapes of energy-loss functions from material to material, that relatively simple analytical formulas cannot accurately represent IMFPs below 200 eV.

SUMMARY

We have calculated IMFPs for 50–2000 eV electrons in 15 inorganic compounds. As we found in similar calculations for a group of 27 elements,[1] there are substantial differences in the shapes of the 1MFP versus energy curves for electron energies below 200 eV. These differences are due to variations in the inelastic electron scattering characteristics of the compounds (as represented by their energy-loss functions).

We have compared the calculated IMFPs for the compounds with values predicted by the TPP-2 formula for predicting IMFPs, which was developed from our IMFP calculations for the elements.[1] The RMS deviation in this comparison was ~23%. We found, however, that the deviation for each compound correlated with uncertainties of the optical data used in the IMFP calculation, as determined by two sum rules. We therefore recommend the use of TPP-2 for calculating IMFPs in these compounds rather than the IMFPs calculated from the optical data. This formula should not be used, however, outside the energy range for which it was developed and tested.

REFERENCES

1. S. Tanuma, C. J. Powell and D. R. Penn, *Surf. Interface Anal.* **17**, 911 (1991).
2. D. R. Penn, *Phys. Rev. B* **35**, 482 (1987).
3. J. Lindhard and M. Scharff, *K. Dan. Vidensk. Selsk. Mat.-Fys. Medd.* **27**, No. 15 (1953); J. Lindhard, M. Scharff and H. E. Schiott, *K. Dan. Vidensk, Selsk. Mat.-Fys. Medd.* **33**, No. 14 (1963); D. Pines, *Elementary Excitations in Solids*, p. 144. W. A. Benjamin, New York (1963).
4. S. Tanuma, C. J. Powell and D. R. Penn, *Surf. Interface Anal.* **11**, 577 (1988).
5. C. J. Powell, *J. Electron Spectrosc.* **47**, 197 (1988).
6. C. J. Powell and M. P. Seah, *J. Vac. Sci. Technol.* **A8**, 735 (1990).
7. A. Jablonski and H. Ebel, *Surf. Interface Anal.* **11**, 627 (1988); A. Jablonski and S. Tougaard, *J. Vac. Sci. Technol.* **A8**, 106 (1990); W. H. Gries and W. Werner, *Surf. Interface Anal.* **16**, 149 (1990); W. S. M. Werner, W. H. Gries and H. Störi, *J. Vac. Sci. Technol.* **A9**, 21 (1991); Z.-J. Ding, Ph.D. Thesis, Osaka University (1990); W. S. M. Werner, W. H. Gries and H. Störi, *Surf. Interface Anal.* **17**, 693 (1991).
8. C. J. Powell, in *Electron Beam Interactions with Solids for Microscopy, Microanalysis and Microlithography*, ed. by D. F. Kyser, H. Niedrig, D. E. Newbury and R. Shimizu, p. 19. Scanning Electron Microscopy, Chicago (1984).
9. H.-J. Hagemann, W. Gudat and C. Kunz, Deutsches Elektronen-Synchrotron Report SR-74/7, Hamburg (1974), unpublished; H.-J. Hagemann, W. Gudat and C. Kunz, *J. Opt. Soc. Am.* **65**, 742 (1975).
10. B. L. Henke, P. Lee, T. J. Tanaka, R. L. Shimabukuro and B. K. Fujikawa, in *Low-Energy X-Ray Diagnostics*, ed. by D. T. Attwood and B. L. Henke, p. 340, Am. Inst. Phys. Conf. Proc. No. 75. American Institute of Physics, New York (1981); *At. Data Nucl. Data Tables* **27**, 1 (1982).
11. *Handbook of Optical Constants of Solids*, ed. by E. D. Palik. Academic Press, New York (1985).
12. E. B. Saloman, J. H. Hubbell and J. H. Scofield, *At. Data Nucl. Data Tables* **38**, 1 (1988).
13. D. Y. Smith, in *Handbook of Optical Constants of Solids*, ed. by E. D. Palik, p. 35. Academic Press, New York (1985).
14. J. Daniels, C. V. Festenberg, H. Raether and K. Zeppenfeld, *Springer Tracts Mod. Phys.* **54**, 77 (1970).
15. D. Pines and P. Nozieres, *The Theory of Quantum Liquids*, Vol. 1, p. 210. W. Benjamin, New York (1966).
16. G. D. Mahan, *Many-Particle Physics*, p. 460. Plenum Press, New York (1981).
17. E. D. Palik, in *Handbook of Optical Constants of Solids II*, ed. by E. D. Palik, p. 3. Academic Press, New York (1991).
18. S. Tanuma, C. J. Powell and D. R. Penn (to be published in *Acta Physica Polonica*).
19. H. Bethe, *Ann. Phys.* **5**, 325 (1930).

20. M. Inokuti, *Rev. Mod. Phys.* **43**, 297 (1971).
21. J. C. Ashley, *J. Electron Spectrosc.* **46**, 199 (1988).
22. J. Szajman and R. C. G. Leckey, *J. Electron Spectrosc.* **23**, 83 (1981); J. C. Ashley, *J. Electron Spectrosc.* **28**, 177 (1982).
23. J. Szajman, J. Liesegang, J. G. Jenkin and R. C. G. Leckey, *J. Electron Spectrosc.* **23**, 97 (1981).
24. C. J. Powell, *Surf. Interface Anal.* **10**, 349 (1987); *Ultramicroscopy* **28**, 24 (1989).
25. D. Y. Smith, E. Shiles and M. Inokuti, in *Handbook of Optical Constants of Solids*, ed. by E. D. Palik, p. 369. Academic Press, New York (1985).
26. *CRC Handbook of Chemistry and Physics*, ed. by R. C. Weast and D. R. Lide, pp. B-68 and E-110. CRC Press, Boca Raton, FL (1989/90); H. P. R. Frederikse, in *American Institute of Physics Handbook*, ed. by D. E. Gray, p. 9–16. McGraw Hill, New York (1972).
27. C. M. Wolfe, N. Holonyak and G. E. Stillman, *Physical Properties of Semiconductors*, p. 340. Prentice Hall, Englewood Cliffs, NJ (1989); N. W. Ashcroft and N. D. Mermin, *Solid State Physics*, p. 566. Holt, Rinehart, and Winston, New York (1976); C. Kittel, *Introduction to Solid State Physics*, p. 210. Wiley, New York (1976).
28. J. C. Ashley and V. E. Anderson, *J. Electron Spectrosc.* **24**, 127 (1981); *IEEE Trans. Nucl. Sci.* **NS-28**, 4132 (1988).
29. J. C. Ashley and C. J. Tung, *Surf. Interface Anal.* **4**, 52 (1982).
30. T. Reich, V. G. Yarzhemski and V. I. Nefedov, *J. Electron Spectrosc.* **46**, 255 (1988).
31. R. Flitsch and S. I. Raider, *J. Vac. Sci. Technol.* **12**, 305 (1975).
32. G. Leonhardt and H. J. Bilz, *Krist. Tech.* **10**, K35 (1975).
33. J. M. Hill, D. G. Royce, C. S. Fadley, L. F. Wagner and F. J. Grunthaner, *Chem. Phys. Lett.* **44**, 225 (1976).
34. M. F. Ebel and W. Lieble, *J. Electron Spectrosc.* **16**, 463 (1979).
35. A. Ishizaka, S. Iwata and Y. Kamigaki, *Surf. Sci.* **84**, 355 (1979).
36. T. Hattori and T. Nishina, *Surf. Sci.* **86**, 555 (1979).
37. R. P. Vasquez and F. J. Grunthaner, *Surf. Sci.* **99**, 681 (1980).
38. M. F. Hochella and A. H. Carim, *Surf. Sci.* **197**, L260 (1988).
39. J. F. Fulghum and G. E. McGuire, personal communication (1988).
40. J. C. Shelton, *Surf. Sci.* **44**, 305 (1974).